

## Quadratic Programming in Control of Brushless Motors

**F. Aghili**  
Canadian Space Agency  
Space Technologies  
Saint-Hubert, J3Y 8Y9  
farhad.aghili@space.gc.ca

**M. Buehler**  
McGill University  
Dept. of Mechanical Engineering  
Montréal, QC H3A 2A7  
buehler@cim.mcgill.ca

**J. M. Hollerbach**  
University of Utah  
Dept. of Computer Science  
Salt Lake City, UT 84112  
jmh@cs.utah.edu

### Abstract

A new torque control strategy for brushless motors with minimum torque ripple and minimum copper losses while maintaining the phase currents under magnetic (or current) saturation is presented. The optimal control – a nonlinear map from desired torque and position to the motor's phase currents – is the closed form solution to a quadratic programming problem. Experimental results demonstrate virtually ripple-free torque and improved tracking accuracy. In case of magnetic or current saturation, the maximum torque capability of the motor is considerably increased.

## 1 Introduction

Modern direct-drive motors are multi-dimensional nonlinear systems. Phase voltages and joint angle are typically considered as the system input and output leading to a complex nonlinear input-output dynamical behavior. Feedback linearization methods [6, 15, 13], singular perturbation techniques [11], and adaptive schemes have been proposed for the control of such systems. Shouse *et al.* [12, 11] presented a self-tuning controller for permanent-magnet synchronous motors, providing for either velocity or position tracking. Taylor [14] applied a digital reduced-order modeling to velocity control design for permanent-magnet synchronous motors minimizing copper losses.

If we consider the motor's phase currents as the inputs in place of the armature voltages, the control problem is reduced to the torque control of motors – a nonlinear map from desired torque to phase currents. Control approaches for accurate torque production in direct drive systems and their underlying models have been studied by several researchers [9, 16, 4, 13]. Murai *et al.* [10] proposed heuristic commutation for non-sinusoidal flux distribution. Le-Huy *et al.* [8, 3] re-

duces the torque ripple harmonics for brushless DC motor by using several drive current waveforms. Ha *et al.* [5] characterized the whole class of ripple-free torque controller that enable the motor to behave like a linear system. Contrary to these past approaches, the proposed controller does not rely on a dynamical model of the system or on any condition for the phase torque-angle waveforms. In summary, the main contribution of this paper is the design of a ripple-free torque controller which minimizes copper losses and maximizes the motor's torque capability under magnetic saturation or current limitation. These claims are validated experimentally on the McGill/MIT direct drive motor [2].

## 2 Optimal Phase Current

### 2.1 Motor Model

The torque  $\tau$  of a motor with  $n$  phases is the superposition of all phase torque contributions,

$$\tau = \sum_{j=1}^n x_j(\theta, \tau_d) a_j(\theta), \quad (1)$$

where  $a_j(\theta)$  and  $x_j(\theta, \tau_d)$  are the  $j$ th phase torque-current shape function and  $j$ th phase current,  $\theta$  is motor angle, and  $\tau_d$  is the desired torque. We have assumed negligible phase torque cross-coupling and reluctance torque. In addition, we assume that the phase currents can be controlled accurately and instantaneously so that the phase currents can be treated as the control inputs.

The torque control problem is to solve the above equation in terms of currents,  $x_j(\theta, \tau_d)$ , as a function of motor position, given a desired motor torque. Equation 1 permits infinitely many (position dependent) phase current waveforms. Since the continuous mechanical

power output of electrical motors is limited primarily by heat generated from internal copper losses, it makes sense to use this freedom to minimize power losses,

$$P_{loss} = R \sum_{j=1}^n x_j^2(\theta, \tau_d), \quad (2)$$

where  $R$  is the armature resistance. Magnetic saturation is another key limitation which should be considered. If  $x_{max} > 0$  is the current limit of the servo-amplifier or the maximum phase current corresponding to magnetic saturation then the phase currents must satisfy

$$|x_j| \leq x_{max} \quad \forall j \in \mathcal{J} = \{1, 2, \dots, n\}. \quad (3)$$

## 2.2 Quadratic Programming

In order to derive the optimal phase currents  $x_j^*(\theta, \tau_d)$  which generate the desired torque (1) and minimize the power losses (2) subject to constraint (3) we need the torque functions  $a_j(\theta)$ . Let the functions be represented at finite numbers of positions. Then, the values at other positions can be found via interpolation. Hereafter, we omit the argument  $\theta$  for simplicity. Now, by setting  $\tau = \tau_d$  in (1), the problem of finding optimal phase currents that minimize power losses, subject to the constraints is formulated as

$$\min f(\mathbf{x}) = x_1^2 + x_2^2 + \dots + x_n^2 \quad (4)$$

$$h(\mathbf{x}) = a_1 x_1 + a_2 x_2 + \dots + a_n x_n - \tau_d = 0 \quad (5)$$

$$g_j(\mathbf{x}) = |x_j| - x_{max} \leq 0, \quad j \in \mathcal{J} \quad (6)$$

where  $\mathbf{x} = [x_1, x_2, \dots, x_n]^T \in \mathfrak{R}^n$  is the vector of design variables. The above is a quadratic programming problem. Since all the functions are convex, any local minimum is a global minimum as well. Now we seek the minimum point  $\mathbf{x}^* = [x_1^*, x_2^*, \dots, x_n^*]^T$  satisfying the equality and inequality constraints. First, however, we exclude the trivial solution  $x_j^* = 0$ . If the  $j$ th torque shape function is zero, that phase contributes no torque regardless of its current,

$$a_j = 0 \implies x_j^* = 0 \quad \forall j \in \mathcal{J}$$

which immediately specifies the optimal phase currents at the crossing point. By excluding the trivial solution,  $x_j^* = 0$ , we obtain a smaller set of variables and number of equations. Therefore, we have to find the optimal solution corresponding to the nonzero part. Hereafter, without loss of generality, we assume that all torque shape functions are non-zero.

If we define

$$\mathcal{L}(\mathbf{x}) = f(\mathbf{x}) + \lambda h(\mathbf{x}) + \vec{\mu}^T \mathbf{g}(\mathbf{x}) \quad (7)$$

the optimal point can be found via the Kuhn-Tucker theorem as follows.

**Theorem 1** [7] *Let  $\mathbf{x}^*$  provide a local minimum of  $f(\mathbf{x})$  satisfy the equality and inequality constraints  $h(\mathbf{x}) \in \mathfrak{R}$ , and  $\mathbf{g}(\mathbf{x}) = [g_1(\mathbf{x}), g_2(\mathbf{x}), \dots, g_n(\mathbf{x})]^T \in \mathfrak{R}^n$ . Assuming that vectors  $(\partial g_j / \partial \mathbf{x})^T|_{\mathbf{x}=\mathbf{x}^*}$ , ( $j \in \mathcal{J}$ ) are linearly independent, then there exist  $\lambda \in \mathfrak{R}$  and  $\vec{\mu} = [\mu_1, \mu_2, \dots, \mu_n]^T \geq 0 \in \mathfrak{R}^n$  such that*

$$\nabla_{\mathbf{x}} \mathcal{L}(\mathbf{x}^*) = 0 \quad (8)$$

$$\nabla_{\lambda} \mathcal{L}(\mathbf{x}^*) = 0 \quad (9)$$

$$\vec{\mu}^T \mathbf{g}(\mathbf{x}^*) = 0. \quad (10)$$

Let  $\text{sgn}(\cdot)$  represents the sign function, where

$$\text{sgn}(x) = \frac{d}{dx}|x| \quad \text{and} \quad x \neq 0.$$

Then  $\nabla_{\mathbf{x}} \mathbf{g}(\mathbf{x}^*) = \text{diag}\{\text{sgn}(x_1^*), \text{sgn}(x_2^*), \dots, \text{sgn}(x_n^*)\}$  is a diagonal matrix whose columns,  $(\partial g_j / \partial \mathbf{x})^T$  are linearly independent. The only pitfall is  $x_j^* = 0$  where the sign function is indefinite. We assume that the optimal current solution associated with the  $j$ th phase,  $x_j^*$  is non-zero if the value of the corresponding shape function,  $a_i \neq 0$ , is non-zero. This assumption will be relaxed later.

Now, substituting  $f(\mathbf{x})$ ,  $h(\mathbf{x})$  and  $\mathbf{g}(\mathbf{x})$  from (4), (5) and (6) into (8), (9), and (10), we obtain

$$2 \begin{bmatrix} x_1^* \\ x_2^* \\ \vdots \\ x_n^* \end{bmatrix} + \lambda \begin{bmatrix} a_1 \\ a_2 \\ \vdots \\ a_n \end{bmatrix} + \begin{bmatrix} \mu_1 \text{sgn}(x_1) \\ \mu_2 \text{sgn}(x_2) \\ \vdots \\ \mu_n \text{sgn}(x_n) \end{bmatrix} = \mathbf{0} \quad (11)$$

$$a_1 x_1^* + a_2 x_2^* + \dots + a_n x_n^* - \tau_d = 0 \quad (12)$$

$$\mu_j (|x_j^*| - x_{max}) = 0 \quad j \in \mathcal{J}. \quad (13)$$

Equations (11), (12), and (13) constitute a set of  $2n+1$  nonlinear equations with  $2n+1$  unknowns  $\mathbf{x}^*$ ,  $\lambda$ , and  $\vec{\mu}$  to be solved as follows. Since  $\vec{\mu} \geq 0$  and  $\mathbf{g}(\mathbf{x}^*) \leq 0$ , equation (10) implies that  $\mu_i = 0$  for  $|x_j| < x_{max}$ , and that  $\mu_j \geq 0$  for  $|x_j| = x_{max}$ . Therefore, (11) can be written concisely as

$$T(x_j^*) = -0.5\lambda a_j \quad j \in \mathcal{J}. \quad (14)$$

In the above, the mapping  $T : \mathcal{D} \mapsto \mathfrak{R}$ , where  $\mathcal{D}(x) = \{x \in \mathfrak{R} : |x| \leq x_{max}\}$ , is defined by

$$T(x) = \begin{cases} x & |x| < x_{max} \\ x + 0.5\text{sgn}(x)\mu & |x| = x_{max} \end{cases} \quad (15)$$

where  $\mu$  is any positive number. Since this map is invertible on  $\mathcal{D}$ , there exists a function  $T^{-1}(T(x)) = x \quad \forall x \in \mathcal{D}$ . Thus,  $x_j^*$  in (14) can be determined uniquely if the right-hand-side of the equation is given.

The inverse of the mapping is the saturation function, i.e.  $T^{-1}(\cdot) \equiv \text{sat}(\cdot)$ , defined by

$$\text{sat}(x) = \begin{cases} x & |x| \leq x_{max} \\ \text{sgn}(x)x_{max} & \text{otherwise} \end{cases} \quad (16)$$

and  $x_{max} > 0$ . Now, (14) can be rewritten as

$$x_j^* = \text{sat}(-0.5\lambda a_j) \quad j \in \mathcal{J} \quad (17)$$

implying that  $x_j^* \neq 0$  as  $a_j \neq 0$ , thus relaxing the assumption made earlier. The second result is that the larger the magnitude of the torque shape function  $|a_j|$ , the larger the magnitude of the optimal current  $|x_j^*|$ . If the phases are labeled in descending order,

$$|a_1| \geq \dots \geq |a_n| \implies |x_1^*| \geq \dots \geq |x_n^*|, \quad (18)$$

the optimal phase currents from  $x_1^*$  to  $x_n^*$  must be saturated consecutively. We shall use this fact to calculate the optimal phase currents consecutively in the same order. Let's first calculate  $x_1^*$ . In the case that saturation of a phase occurs, (17) implies that only knowing the sign of  $\lambda$  is enough to calculate the associate phase current. One can infer from (14) and (12) that  $\text{sgn}(\tau_d) = \text{sgn}(-\lambda)$ . Therefore, if  $x_j^*$  reaches its saturation limit, then

$$x_1^* = \text{sgn}(-a_1\lambda)x_{max} = \text{sgn}(a_1\tau_d)x_{max}. \quad (19)$$

In contrast, if  $x_1^*$  does not saturate, i.e.  $|x_1^*| < x_{max}$ , then neither does  $\{x_2, \dots, x_n\}$ , according to (18). Let  $\lambda^{(1)}$  represent the Lagrangian multiplier when  $x_1^*$  does not saturate, then the Lagrangian multiplier can be calculated by substituting phase currents from  $x_j^* = -0.5\lambda a_j$  into (12)

$$\lambda^{(1)} = \frac{-2\tau_d}{\sum_{i=1}^n a_i^2} \quad (20)$$

which, in turn, can be substituted in (17) to obtain the optimal phase current

$$x_1^* = \text{sat}\left(\frac{a_1\tau_d}{\sum_{k=1}^n a_k^2}\right). \quad (21)$$

Since the denominator in (21) is always positive, by virtue of (19), one can infer that (21) also provides the optimal solution for the saturation case too. Analogously,  $x_2^*$  can be calculated if  $a_1x_1^* - \tau_d$  is treated as the known parameter in (12). In general, the  $i$ th phase current can be calculated by induction as follows: assume that upto  $(i-1)$ th phase currents have been solved, then we have

$$\underbrace{a_1x_1^* + \dots + a_{i-1}x_{i-1}^*}_{\text{known}} + \underbrace{a_ix_i^* + \dots + a_nx_n^*}_{\text{unknown}} - \tau_d = 0. \quad (22)$$

The Lagrangian multiplier associated with the case of unsaturated  $x_i^*$  can be found from (17) and (22) as

$$\lambda^{(i)} = \frac{-2(\tau_d - \sum_{k=1}^{i-1} a_k x_k^*)}{\sum_{k=i}^n a_k^2}. \quad (23)$$

Substituting (23) in (17), gives

$$x_i^* = \text{sat}\left(\frac{a_i\tau_d - a_i \sum_{k=1}^{i-1} a_k x_k^*}{\sum_{k=i}^n a_k^2}\right), \quad i = 2, \dots, n. \quad (24)$$

### 3 Maximum Attainable Torque

The control algorithm presented above permits torque sharing among phases when one phase saturates. It is of interest to know how much torque is gained using this method. One can show that the optimal solution of phase current without taking the saturation into account can be expressed explicitly in closed form as

$$x_j(\theta, \tau_d) = \frac{a_j(\theta)\tau_d}{a_1^2(\theta) + a_2^2(\theta) + \dots + a_n^2(\theta)} \quad \forall j \in \mathcal{J}. \quad (25)$$

In this case, the maximum torque depends on the saturation of the largest phase torque function. It is clear from (25) that the phase with the largest  $|a_j|$  reaches the saturation first. Again, assuming that  $|a_1| \geq |a_2| \geq \dots \geq |a_n|$ , then the maximum achievable torque can be calculated from (25)

$$\frac{|\tau_d|}{x_{max}} \leq (|a_1| + |a_2/a_1||a_2| + \dots + |a_n/a_1||a_n|) = k_1(\theta). \quad (26)$$

On the other hand, our proposed algorithm allows us to demand more torque as the burden of the shared torque is shifted to unsaturated phases when one phase saturates. Obviously, this can go on until all phases have saturated. Hence the maximum magnitude torque satisfies

$$\frac{|\tau_d|}{x_{max}} \leq (|a_1| + |a_2| + \dots + |a_n|) = k_2(\theta). \quad (27)$$

$k_1(\theta) > 0$  and  $k_2(\theta) > 0$  are important factors in the torque capability of motors. Since  $|a_2/a_1| \leq 1, \dots, |a_n/a_1| \leq 1$ , one can conclude from (26) and (27) that  $k_1(\theta) \leq k_2(\theta)$ . The values of  $k_1$  and  $k_2$  depend on the shape of the torque functions. However, they can be expressed explicitly for an ideal three-phase motor, i.e.  $n = 3$ , where we have three shifted sinusoidal torque functions as  $a_1(\theta) = \hat{a} \sin(\theta + \varphi)$ ,  $a_2(\theta) = \hat{a} \sin(\theta + 2\pi/3 + \varphi)$ , and  $a_3(\theta) = \hat{a} \sin(\theta + 4\pi/3 + \varphi)$ . In this case, using the properties of triangular functions, one can show

$$\sqrt{3}\hat{a} \leq k_1(\theta) \leq 1.5\hat{a}, \quad 2\hat{a} \leq k_2(\theta) \leq \sqrt{3}\hat{a}.$$

Therefore the maximum torque capability is boosted by  $2/\sqrt{3}$  when the phase saturation is considered in the phase current shape function.

## 4 Experiments

### 4.1 Identification

We measure the torque shape functions experimentally on a hydraulic dynamometer [1]. To this end, the torque trajectory data versus position was logged during the rotation, while one phase was energized with a constant current. Cogging and friction torques act as disturbances to the torque measurement and often are a function of position. For more accurate results, the joint friction and cogging torque are identified and then subtracted from the torque measurement. The cogging torque is due to residual magnetization in the stator armatures, while the friction torque arises in the motor bearings and consists of viscous and dry friction. Since direct-drive motors operate at relatively low speed, dry friction,  $\tau_F$ , dominates. The main problem in identification of the phase torque-angle characteristic is that the dry-friction is position dependent. Let  $\tau_M(\theta)$  and  $\tau_F(\theta)$  represent the motor torque and the magnitude of the dry-friction,

$$\tau_M(\theta) = \tau(\theta) - \tau_F(\theta)\text{sgn}(\dot{\theta}).$$

Suppose  $\tau_M^+$  and  $\tau_M^-$  represent two sequences of torque measurement corresponding to clockwise and counter-clockwise rotations, then the magnetic and friction torque can be readily calculated as

$$\begin{aligned} \tau(\theta) &= \frac{1}{2}[\tau_M^+(\theta) + \tau_M^-(\theta)] \\ \tau_F(\theta) &= \frac{1}{2}[\tau_M^+(\theta) - \tau_M^-(\theta)] \end{aligned} \quad (28)$$

The cogging torque is obtained by setting the phase current to zero. The dry friction, cogging, and the

three phases' torque-angle profiles (with friction and cogging torques subtracted) are illustrated in Fig. 1 where the phase currents are individually set to  $8A$ . Although our experiments showed that friction torque  $\pm 1Nm$  and cogging torques are relatively low, we compensate both friction and cogging torques for a more accurate torque generation.

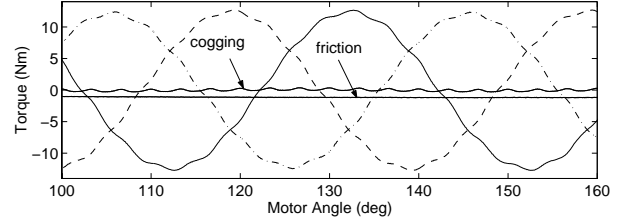


Figure 1: Friction torque, cogging torque and three phase torque-angle profiles.

### 4.2 Implementation of the Torque Control Algorithm

If  $[a_j(\theta_1), a_j(\theta_2), \dots, a_j(\theta_p)] \in \mathbb{R}^p$  represent the discrete torque shape functions corresponding to  $p$  measurements of the phase torque (with unit current excitation) and positions then the torque control algorithm may proceed by the following steps:

1. Read position, and then interpolate the corresponding torque shape functions  $a_j$ .
2. Set  $x_j^* = 0$  for  $a_j = 0$  (or for suff. small  $|a_j|$ ).
3. pick the set of nonzero shape functions and sort them s.th.  $|a_1| \geq |a_2| \geq \dots \geq |a_n|$  and calculate the optimal currents from (21) and (24); go to step 1.

### 4.3 Torque Ripple

The torque controller was tested on the dynamometer. The motor shaft is rotated by the hydraulic actuator while the motor torque is monitored by the torque transducer. Fig. 2 shows a dramatic reduction in torque ripple with our proposed controller compared to sinusoidal commutation.

### 4.4 Torque Saturation

Here we demonstrate how much the maximum torque capability of our motor prototype is enhanced by using our proposed control algorithm. Fig. 3 shows the

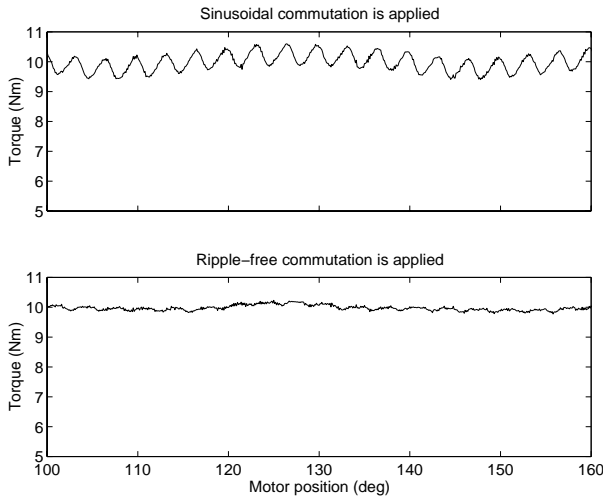


Figure 2: Motor torque in sinusoidal (top) and the ripple free (bottom) commutations.

graphs of the maximum achievable torque with respect to maximum phase current  $x_{max} = 15A$  that are with (solid line) and without (dashed line) consideration of the current saturation in the torque control law. It is evident from the graphs that the motor torque limits corresponding to the torque controllers are  $34Nm$  and  $41Nm$  – an increase of 20% for the proposed torque controller.

One aspect of our proposed torque control algorithm is the current-position pattern varies upon the requested torque. This is demonstrated in Fig. 4 (top) and (bottom) which show the current-position pattern of the motor with respect to the requested torques  $10Nm$  and  $38Nm$ , respectively.

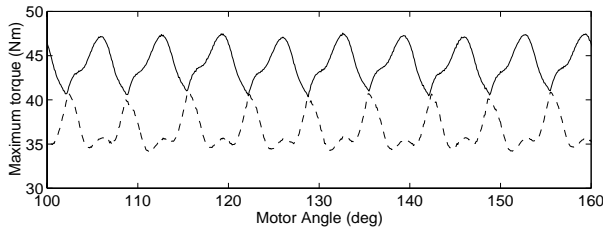


Figure 3: Maximum admissible torque corresponding to maximum phase current  $15A$ . Solid: with torque sharing, dashed: without torque sharing.

#### 4.5 Two Phase Commutation

An interesting aspect of the proposed controller is that it does not rely on any condition on the torque-

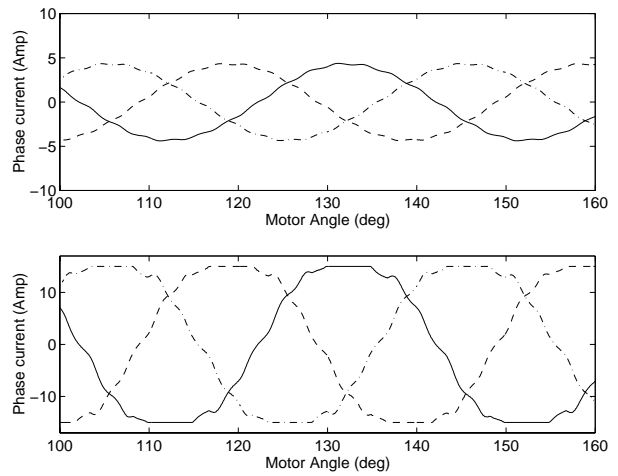


Figure 4: Phase current with the requested torque  $10Nm$  (top), and  $38Nm$  (bottom) respectively.

position pattern of the phases, such as having balanced phases where  $\sum a_j = 0$  [5]. Therefore, the control algorithm can achieve ripple-free torque even if one of the motor phases fails. Fig. 5 shows the phase currents of two phases commutation which produces the same torque  $10 Nm$  produced by three phase commutation Fig. 4 (top). This can be useful in practice when there is need to continue operating the motor even in the case of one phase failure. The penalty is an increase in power consumption, in this particular case from  $75W$  to  $128W$ .

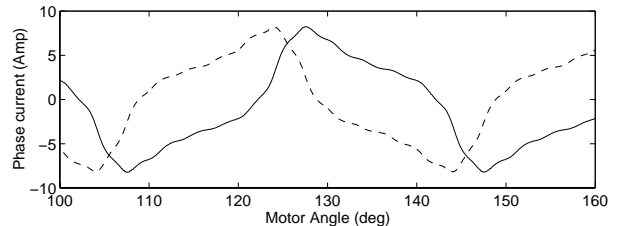


Figure 5: Phase current profile when the motor operates only with two phases.

## 5 Conclusion

The motor torque control problem was interpreted as the optimization of a nonlinear mapping from commanded torque and motor position to commanded phase currents. We have formulated the problem with power losses in winding as the cost function while the torque equation and magnetic (or current) saturation

enter as equality and inequality constraints. The optimal phase current minimizing the copper losses subject to the ripple-free constraint and the phase current saturation constraint has been rigorously solved by the application of the Kuhn-Tucker theorem. The solution is explicitly presented in a form of mapping of the current phases versus torque set-point and position.

A hydraulic dynamometer has been developed to characterize the torque-angle, torque-current characteristics of a direct-drive motor phases. Finally, our torque control algorithm has been implemented in real-time for our direct drive system. Experimental results have demonstrated that torque-ripple is almost eliminated. How much torque ripple affects the accuracy of position controllers has been investigated experimentally. It has been shown that we can achieve 0.003 degree accuracy in position tracking when the proposed commutation is used. We also showed that by considering current (magnetic) saturation in the design of torque control, the maximum torque capability of our motor is boosted by 20%.

## References

- [1] F. Aghili, M. Buehler, and J. M. Hollerbach. Torque ripple minimization in direct-drive systems. In *Proc. IEEE/RSJ Int. Conf. Intelligent Systems and Robots*, pages 794–799, Victoria, BC, Canada, Oct 1998.
- [2] F. Aghili, M. Buehler, and J. M. Hollerbach. Development of a high performance direct-drive joint. In *Proc. IEEE/RSJ Int. Conf. Intelligent Systems and Robots*, Japan, October 2000.
- [3] E. Favre, L. Cardoletti, and M. Jufer. Permanent-magnet synchronous motors: A comprehensive approach to cogging torque suppression. *IEEE Trans. Industry Applications*, 29(6):1141–1149, 1993.
- [4] F. Filicori, C. G. Lo Bianco, and A. Tonielli. Modeling and control strategies for a variable reluctance direct-drive motor. *IEEE Trans. Industrial Electronics*, 40(1):105–115, 1993.
- [5] Ha and Kang. Explicit characterization of all feedback linearizing controllers for a general type of brushless dc motor. *IEEE Trans. Automatic Control*, 39(3):673–677, 1994.
- [6] M. Ilic'-Spong, R. Marino, S. M. Peresada, and D. G. Taylor. Feedback linearizing control of switched reluctance motors. *IEEE Trans. Automatic Control*, AC-32(5):371–379, 1987.
- [7] H. W. Kuhn and A. W. Tucker. Nonlinear programming. In *Proc. Second Berkeley Symposium on Mathematical Statistics and Probability*, pages 481–492, Berkeley: University of California Press, 1951.
- [8] H. Le-Huy, R. Perret, and R. Feuillet. Minimization of torque ripple in brushless dc motor drives. *IEEE Trans. Industry Applications*, pages 748–755, 1986.
- [9] D. G. Manzer, M. Varghese, and J. S. Thorp. Variable reluctance motor characterization. *IEEE Trans. Industrial Electronics*, 36(1):56–63, 1989.
- [10] Y. Murai, Y. Kawase, K. Ohashi, and K. Okuyama. Torque ripple improvement for brushless dc miniature motors. *IEEE Trans. Industry Applications*, 25(3):441–449, 1993.
- [11] Shouse and D. G. Taylor. A digital self-tuning tracking controller for pm synchronous motors. In *IEEE Conf. Decision and Control*, pages 3397–3402, San Antonio, 1992.
- [12] Shouse and D. G. Taylor. Observer based control of pm synchronous motors. In *Int. Conf. Industrial Electronics, Control, Instrumentation and Automation*, pages 1482–1487, San Diego, 1992.
- [13] D. G. Taylor. Nonlinear control of electric machines: An overview. *IEEE Control Systems*, 14(6):41–51, 1994.
- [14] D. G. Taylor. Digital reduced-order modeling and feedback for nonlinear systems. In *Proceedings of workshop on advances in control and its applications*, pages 257–281, New York Springer, 1996.
- [15] D. G. Taylor, M. Ilic'-Spong, R. Marino, and S. Peresada. A feedback linearizing control for direct-drive robots with switched reluctance motors. In *Proc. IEEE Int. Conf. Decision and Control*, Miami Beach, Dec 1986.
- [16] R. S. Wallace and D. G. Taylor. Low-torque-ripple switched reluctance motors for direct-drive robotics. *IEEE Trans. Robotics and Automation*, 7(6):733–742, 1991.